LANGMUIR

pubs.acs.org/Langmuir Article

Effect of Molecular Structure on Electrochemical Phase Behavior of Phospholipid Bilayers on Au(111)

Philip N. Jemmett, David C. Milan, Richard J. Nichols, Liam R. Cox, and Sarah L. Horswell*

Cite This: *Langmuir* 2021, 37, 11887−11899 Read Online

ACCESS | Metrics & More | Article Recommendations | Supporting Information

ABSTRACT: Lipid bilayers form the basis of biological cell membranes, selective and responsive barriers vital to the function of the cell. The structure and function of the bilayer are controlled by interactions between the constituent molecules and so vary with the composition of the membrane. These interactions also influence how a membrane behaves in the presence of electric fields they frequently experience in nature. In this study, we characterize the electrochemical phase behavior of dipalmitoylphosphatidylcholine (DPPC), a glycerophospholipid prevalent in nature and often used in model systems and healthcare applications. DPPC bilayers were formed on Au(111) electrodes using Langmuir−Blodgett and Langmuir−Schaefer deposition and studied with electrochemical methods, atomic force microscopy (AFM) and in situ polarization-modulated infrared reflection absorption spectroscopy (PM-IRRAS). The coverage of the substrate determined with AFM is in accord with that estimated from differential capacitance measurements, and the bilayer thickness is slightly higher than for bilayers of the similar but shorter-chained lipid, dimyristoylphosphatidylcholine (DMPC). DPPC bilayers exhibit similar electrochemical response to DMPC bilayers, but the organization of molecules differs, particularly at negative charge densities. Infrared spectra show that DPPC chains tilt as the charge density on the metal is increased in the negative direction, but, unlike in DMPC, the chains then return to their original tilt angle at the most negative potentials. The onset of the increase in the chain tilt angle coincides with a decrease in solvation around the ester carbonyl groups, and the conformation around the acyl chain linkage differs from that in DMPC. We interpret the differences in behavior between bilayers formed from these structurally similar lipids in terms of stronger dispersion forces between DPPC chains and conclude that relatively subtle changes in molecular structure may have a significant impact on a membrane's response to its environment.

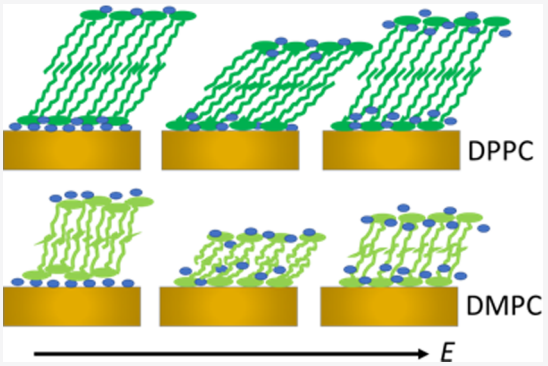

1. INTRODUCTION

Dipalmitoylphosphatidylcholine (DPPC) is one of the most prevalent phospholipids found in nature and is a common constituent of mammalian cell membranes.[1−4] As a result, it has been widely used in many applications, including eye drops,[5−7] synthetic lung surfactants,[8,9] cosmetics, and liposome solutions for drug delivery.[10,11] It has also proved a popular model system for investigating simpler models of biological cell membranes, sometimes as a matrix for the study of membrane proteins, receptors used in sensing, or drug−membrane interactions,[12−15] sometimes to build an understanding at a fundamental level of the behavior of the lipid bilayer that makes up the cell membrane.[16−18] It is increasingly being recognized that the lipid composition of the cell membrane is crucial to function,[19−22] and a range of techniques has been employed to investigate the structures of lipid ensembles, including vesicles, lipid monolayers, stacked lipid bilayers, suspended lipid layers, and supported lipid bilayers.[23,24] For DPPC, data have been collected to determine molecular volume,[25] phase behavior,[26,27] molecule arrangement in monolayers at the air|water interface,[16,28] and thickness of layers in multilayers and monolayers.[29−31] The packing arrangements, numbers of associated water molecules per lipid, and the location of such associated water molecules, in various phases of DPPC, have been characterized,[32] but the influence of static electric field on DPPC has not yet been investigated. One of the roles of a natural membrane is to separate environments within a cell or to separate the intracellular and extracellular environments; in so doing, concentration gradients of ions across the membrane are formed[33] and thus charge separation occurs. This charge separation, or even the charge asymmetry resulting from the asymmetric distribution of lipids in mammalian plasma membranes, results in strong electric fields of up to 10^7 V m^{-1}.[34] Changes in the field across the membrane can result in changes in structure, for example, the reorientation of dipoles

Received: July 25, 2021
Revised: September 10, 2021
Published: September 30, 2021

or even membrane breakdown at high fields,[35] so the study of these changes is essential for understanding the function of the membrane. Electrochemical measurements provide a means to tune an electric field continuously over a similar range to that found in nature[35,36] and have demonstrated the effect of this field on monolayers for various lipids on mercury.[37−48] Further in situ structural studies, utilizing techniques such as atomic force microscopy,[49−53] scanning tunneling microscopy,[54,55] vibrational spectroscopy,[35,49,50,56−62] and neutron reflectivity[36,63,64] to investigate bilayers supported on or floating on gold electrodes, have shown changes in ensemble structure as the applied field is varied. Some studies have highlighted the role of lipid molecule structure on ensemble structure and response to the applied field;[56,61,62] others have focused on the interaction of peptides and proteins with a lipid bilayer and how charge controls their insertion.[52,55,58−60]

In this work, we have employed a combination of techniques to study the structure and response of supported DPPC bilayers to an applied electric field. Dimyristoylphosphatidylcholine (DMPC) behavior has been thoroughly characterized by Lipkowski and co-workers.[35,49−51] DPPC has not yet been studied in this way but is a popular choice in other areas of biomimetic membrane research and merits study because of its prevalence in nature. DPPC differs from DMPC in the length of hydrocarbon chains, which are two carbon-atoms longer (see Figure 1). We find that DPPC bilayers are slightly thicker

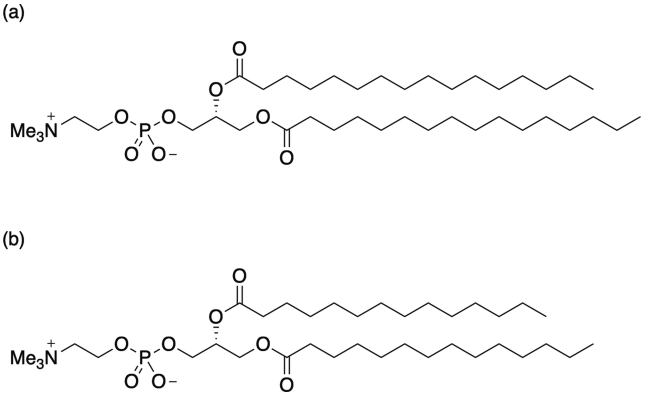

Figure 1. Structures of (a) dipalmitoylphosphatidylcholine (DPPC) and (b) dimyristoylphosphatidylcholine (DMPC). DPPC has acyl chains 16 carbon-atoms long and DMPC has acyl chains 14 carbon-atoms long.

than DMPC bilayers and the apparently small difference in molecular structure leads to different packing and different electrochemical phase behavior. Our findings highlight the role that subtle variations in the molecular structure of lipids play in determining the physicochemical properties of their ensembles and the need to acquire information on a wide range of systems because what may, at first sight, appear to be a minor structural variation can give rise to quite different behavior in biomimetic systems.

2. EXPERIMENTAL SECTION

2.1. Materials. Ultrapure water, purified with a Millipore tandem Elix-MilliQ Gradient A10 system (resistivity ≥ 18 MΩ cm, TOC ≤ 5 ppb), was used throughout. Glassware was cleaned either with piranha solution (*caution! can cause explosion!*) or by heating in a 1:1 mixture of concentrated nitric and sulfuric acids for at least 1 h, in each case followed by rinsing with copious quantities of ultrapure water and soaking in ultrapure water overnight. Kel-F and Teflon parts and viton o-rings were cleaned by soaking in a ∼1:1 mixture of ammonia (35%) solution and hydrogen peroxide (30%) solution for several hours, followed by thorough rinsing with ultrapure water and soaking in ultrapure water overnight. Spectroelectrochemical cell parts were dried in a designated clean oven prior to assembly of the cell.

Lipid solutions were prepared in mixed methanol and chloroform (1:2 ratio) solvent. Both solvents were HPLC grade (Sigma Aldrich). The lipid used in this work, dipalmitoylphosphatidylcholine (DPPC), was purchased from Avanti Polar Lipids and used as received. The sodium fluoride used to prepare electrolyte solutions was Premion grade (Alfa) and used as received. Electrolyte solutions were prepared as 0.1 M aqueous solutions.

2.2. Langmuir Trough Measurements. A Teflon Langmuir trough, with dipper and Delrin barrier (Nima), was used to record isotherms and to deposit lipid bilayers on gold substrates. The trough was cleaned with chloroform, then water was added, and its surface checked for cleanliness by monitoring the surface pressure over the entire available area. 70 μL of a 1 mg mL^{-1} solution of DPPC was deposited on the water surface and the solvent was allowed to evaporate. Isotherms were recorded with the barrier speed set to 25 cm^2 min^{-1} (available trough area ∼600 cm^2). A typical isotherm is presented in Figure S1. Its shape and limiting molecular area are consistent with literature reports.[65,66] The isotherm indicates that several phases can be formed: a liquid expanded (L_e) phase is observed at a high area per molecule and condenses on compression to form a liquid condensed (L_c) phase. The limiting molecular area (defined by the extrapolation of the L_c region to the area axis) is around 50 Å^2, very close to that measured in our laboratory under the same conditions for DMPC.[67] As may be expected from the geometry of the two molecules, the limiting area per molecule is determined by the size of the PC headgroup. Y-type lipid bilayers were formed on clean gold electrodes or gold-on-glass slides using Langmuir−Blodgett deposition followed by Langmuir−Schaefer (horizontal touch) deposition (LB−LS deposition). The cleaned gold substrates were placed in the water subphase prior to deposition of the lipid monolayer. The substrate was then withdrawn vertically through the interface at a controlled surface pressure of 40 mN m^{-1} at a rate of 2 mm min^{-1}, then dried in argon for 30 min before the Langmuir−Schaefer deposition was performed. At this surface pressure, the lipid monolayer is in the L_c phase, and the area per molecule is ∼45 Å^2.

2.3. Electrochemical Measurements. Electrochemical measurements were carried out in a standard all-glass three-electrode cell, connected to a reference electrode compartment through a salt bridge. The reference electrode was a saturated calomel electrode (SCE, Hach Lange GmbH), and the counter electrode was a gold coil, which was flame-annealed and quenched with ultrapure water before being placed in the cell. The working electrode was a Au(111) sample, oriented to better than 0.5° (MaTecK GmbH, Germany). It was cleaned by flame-annealing as described in the literature[68] and transferred to the electrochemical cell with a drop of ultrapure water. The electrolyte used was 0.1 M NaF and was deoxygenated before measurements by bubbling with argon gas. An argon atmosphere was maintained above the solution throughout the experiment. The electrochemical response of the clean system was checked before depositing a bilayer on the surface. (N.B. The Au(111) surface is reconstructed on flame-annealing and, as the electrolyte does not contain strongly adsorbing species, the surface may be assumed to remain reconstructed over the potential range studied.)

Chronocoulometry experiments were performed with a Heka PGSTAT590 potentiostat, controlled with in-house written software via a data acquisition board (National Instruments). The software used to acquire the data was kindly provided by Dr. Alexei Pinheiro (Universidade Tecnologica Federal do Parana, Londrina, Brazil). The measurements consisted of applying a series of potential steps, as described in previous publications.[35,61] The potential was held at a base potential of −0.1 V before being stepped to the potential of interest. The potential of interest was maintained for a period of 3 min to allow equilibrium to be established, then stepped for 0.15 s to a potential that is sufficiently negative to desorb the lipids, and then returned to the base potential for 1 min. The process was repeated for

https://doi.org/10.1021/acs.langmuir.1c01975
Langmuir 2021, 37, 11887−11899

a series of potentials, stepping in the negative direction in increments of 0.05 V. During the step to the desorption potential, a current transient was recorded. Each current transient was integrated to give the total charge passed during the potential step. These relative charge densities can then be converted to absolute charge densities, knowing the potential of zero charge of the electrode.

2.4. Atomic Force Microscopy Measurements. Bilayers were deposited on gold-on-glass slides for AFM measurements. These 11 mm × 11 mm glass slides were obtained from Arrandee (Westfalen, Germany) and consisted of glass coated with a 2.5 nm adhesion layer of chromium and a 250 nm layer of gold. These were briefly flame-annealed, cooled, and transferred with a drop of water to the Langmuir trough for deposition. After flame-annealing, the surface recrystallizes to give (reconstructed) (111)-structured microcrystalline regions,[69] which are used for imaging experiments. The AFM measurements were performed with a Nanoscope IIIA (Digital Instruments). Measurements were carried out in air in tapping mode with Au NT-MDT cantilevers (CSG30, Golden Silicon Probes). The nominal resonant frequency was 48 kHz, which was then calibrated to find the AC tuning resonant frequency of 39 kHz. The nominal force constant of the tips was 0.6 N m^{-1}, and cantilever-tip assemblies were calibrated to give a value of 0.308 N m^{-1}.

2.5. Infrared Measurements. Infrared measurements were carried out with a Bruker Vertex 80v spectrometer equipped with an external PMA50 module that comprised a photoelastic modulator (PEM-100, Hinds Instruments), with a ZnSe 50 kHz optical head, and a synchronous sampling demodulator (GWC Technologies). Data were collected with an MCT detector (cooled with liquid nitrogen) at a resolution of 2 cm^{-1}. Transmission spectra were measured to enable the calculation of isotropic optical constants of DPPC in H_2O and in D_2O. These spectra were recorded using a demountable liquid cell (PIKE Technologies, Madison) with BaF_2 windows and a 25 μm spacer. Typically, 0.1 M NaF (in H_2O or D_2O) was used for both analyte solution and background to suppress the dissolution of the BaF_2 windows. Optical constants were calculated from these spectra using software kindly provided by Dr. Vlad Zamlynny (Acadia University, Canada)[70] and subsequently used to simulate PM-IRRA spectra of randomly oriented molecules, which are needed to calculate the orientations of transition dipole moments from experimental PM-IRRA spectra (vide infra).

Spectroelectrochemical measurements were performed with a custom-built cell. A BaF_2 1″ equilateral prism (Crystran, U.K.) was used as the window. The working electrode was a Au(111) single crystal (99.999% purity, orientation < 0.5°, MaTeck, Germany), also cleaned by flame-annealing before deposition of the lipid bilayer. The counter electrode was a gold coil (99.999%, Alfa Aesar), arranged concentric to the working electrode. The reference electrode was a Ag|AgCl|3 M KCl electrode (BASi) and was connected to the cell via a tube placed as close to the working electrode as possible. All potentials in this work are reported with respect to the Ag|AgCl electrode. The electrolyte used in the cell was 0.1 M NaF (Premion grade, Alfa Aesar) in either ultrapure water (for investigating the phosphate stretching region) or in deuterium oxide (for investigating the C−H and C═O stretching regions). Spectra were collected at 19 °C (±1 °C).

The PEM was set for half-wave retardation at 2900 cm^{-1} for studying the C−H stretching region, at 1600 cm^{-1} for studying the C═O stretching region, and at 1100 cm^{-1} for studying the phosphate stretching region. The signal obtained depends on the angle of incidence of the infrared light and the thickness of the gap between the sample and the window. The values of angles of incidence and gap thickness for optimum signal were chosen using the values calculated by Zamlynny.[71] These values are 51° and 2 μm at 2900 cm^{-1}, 60° and 3.5 μm at 1600 cm^{-1}, and 57° and 2 μm at 1100 cm^{-1}. Thicknesses were calculated by comparing reflectivity spectra with the theoretical reflectivity spectra simulated for the cell configuration.[72] This procedure was carried out with "Fresnel 1" software kindly provided by Dr. Vlad Zamlynny.[70]

3. RESULTS AND DISCUSSION

3.1. Electrochemical Results. Figure 2a presents the differential capacity curve obtained for a DPPC-coated

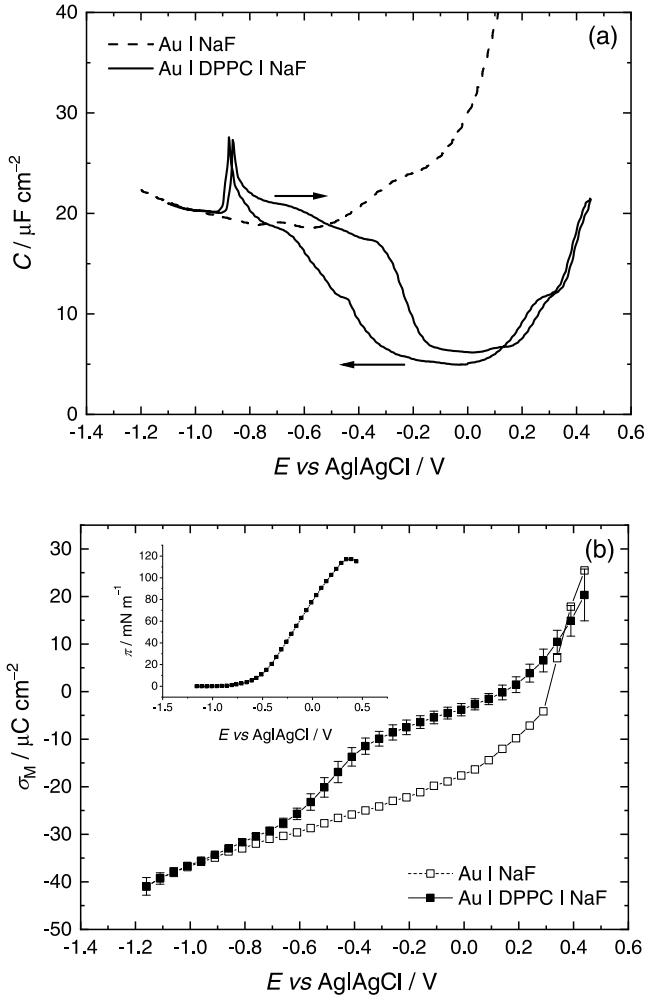

Figure 2. (a) Differential capacitance for Au(111) in 0.1 M NaF (dashed line) and Au(111) with an LB−LS bilayer of DPPC in 0.1 M NaF electrolyte (solid line). Potential sweep rate 5 mV s^{-1}, frequency 20 Hz, and amplitude 5 mV. (b) Chronocoulometry data for Au(111) in 0.1 M NaF (open squares) and for Au(111) with an LB−LS bilayer of DPPC in 0.1 M NaF (filled squares). Inset: surface pressure vs potential for Au(111) with a bilayer of DPPC.

Au(111) electrode in 0.1 M NaF solution. The curve merges with that obtained for uncoated Au(111) in the same solution at potentials negative of −0.9 V, which indicates desorption of the DPPC bilayer at these potentials. A peak in the capacitance at −0.87 V arises from adsorption (in the positive-going scan) or desorption (in the negative-going scan) of DPPC. In the positive sweep, the peak is followed by a gradual decrease in capacity between −0.8 and −0.3 V until a sharper decrease between −0.3 and −0.1 V, where a minimum is reached. By analogy with previous reports on similar molecules,[35,36,56,61,62] this step is likely to result from a change in phase from a bilayer adsorbed on a water layer negative of around −0.4 V to a bilayer directly adsorbed on Au positive of −0.4 V. The hysteresis between the positive-going and negative-going scans indicates slow kinetics for this phase transition. At more positive potentials, an increase in capacity occurs, which may

https://doi.org/10.1021/acs.langmuir.1c01975
Langmuir 2021, 37, 11887−11899

relate to reorientation of molecules, to submonolayer oxidation of gold in regions where there are defects in the film or to the onset of desorption of molecules. The minimum capacity is ~8 μF cm^{-2} on the positive-going sweep and ~5 μF cm^{-2} on the negative-going sweep. These values are similar to those measured for films formed from DMPC[51] and higher than that measured for DMPE LB−LS bilayers.[61] They can be used to estimate surface coverage by comparison with the capacities of a perfect film and of a bare electrode surface, according to eq 1

$$C = \frac{C_0 - C}{C_0 - C_1} \quad (1)$$

where C is the measured capacity and C_0 and C_1 are the capacities of the interface where the electrode surface is covered with no film and with the film in the absence of defects, respectively.[73] At 0 V, C is 5 μF cm^{-2} and C_0 is 27 μF cm^{-2}. If C_1 is taken to be 0.8 μF cm^{-2} (half the capacity of a Hg electrode coated in a monolayer of lipids[74]), a coverage of Au(111) with DPPC of 84% can be estimated. Below, we shall see that this value is consistent with estimates of coverage using AFM measurements.

Figure 2b presents plots of surface charge density as a function of applied potential, obtained with chronocoulometry, for a Au(111) electrode in 0.1 M NaF in the absence and presence of an adsorbed bilayer of DPPC. The shape of the plot acquired with a DPPC bilayer resembles those obtained previously for other phospholipids.[35,61,62] The molecules are adsorbed on the Au(111) surface over an applied potential range of 0.4 to −0.4 V. A phase transition to another adsorbed state takes place at −0.4 V, and for potentials negative of −0.9 to −0.95 V, the bilayer is completely desorbed. These states have been previously assigned for the related phospholipid, DMPC, as a directly adsorbed bilayer at small charge densities (the positive potential range) and a bilayer adsorbed on an electrolyte cushion at larger, negative charge densities.[36,63] At high charge densities, the electric field is strong and the interaction of solvent dipoles (and ions) with the field is increased. The resemblance of the electrochemical data presented here to those acquired for other phospholipids suggests that the electrochemical phase behavior is very similar. A small negative shift of −0.16 V in the potential of zero charge (pzc) is observed, consistent with those observed for other zwitterionic phospholipids (within error—the step size is 50 mV).[35,61,75] The shift is related to a small overall dipole moment normal to the surface, which arises from an asymmetry in the charge distribution across the bilayer.[35] A similar shift in pzc to that observed for other zwitterionic lipids (DMPC[35,75] and DMPE[61,75]) would suggest that the orientations of headgroups in the two monolayers and the quantity of displaced water are comparable.

The area between the charge density plots yields the surface pressure, π, according to eq 2

$$\pi = \gamma_0 - \gamma = \int_{E=-1.15\ \mathrm{V}}^{E} \sigma_{\mathrm{M}}\, \mathrm{d}E - \int_{E=-1.15\ \mathrm{V}}^{E} \sigma_{\mathrm{M}_0}\, \mathrm{d}E \quad (2)$$

where γ_0 and γ are specific surface energies and σ_{M_0} and σ_{M} are charge densities in the absence and presence of the bilayer, respectively.[76] The surface pressure obtained from the charge densities is plotted vs potential in the inset to Figure 2b. A classic bell-shaped plot is observed, with its maximum at the pzc, typical for the adsorption of neutral molecules. The maximum surface pressure is ~118 mN m^{-1}, approximately twice the collapse pressure of DPPC monolayers and close to the value obtained for DMPE bilayers on Au(111).[61]

3.2. AFM Measurements. The quantitative analysis of PM-IRRA spectra relies on the simulation of spectra of randomly oriented molecules in a film of the same thickness so AFM measurements were carried out to determine the film thickness of DPPC bilayers on the Au surface. Figure 3 shows

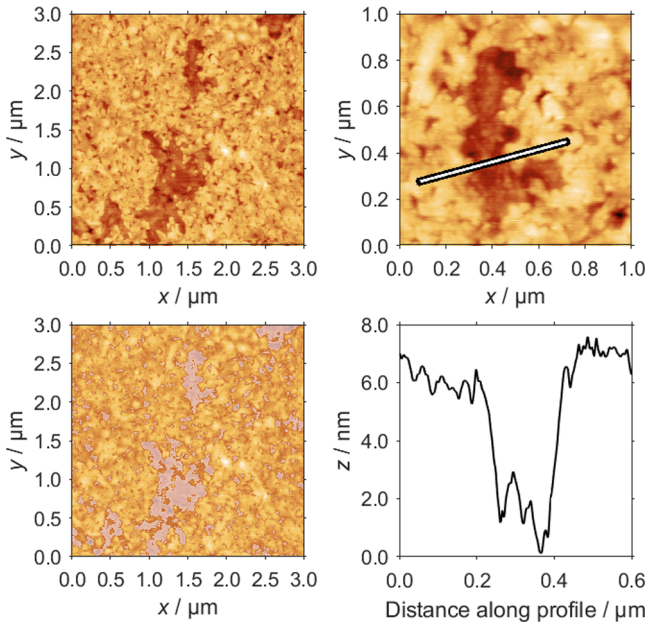

Figure 3. Representative AFM image of a DPPC bilayer on a gold-on-glass slide. Top left: a large-scale image showing typical topography of a DPPC bilayer on a glass|Au slide. Bottom left: the same image with a false color overlay representing the areas of the slide that are not covered with the DPPC layer. Top right: a smaller-scale image focused on an area of low coverage with a depth profile measured across that defect shown in a thick white line. Bottom right: the z-axis deflection of the cantilever across the profile marked in the top right image.

AFM images, obtained in noncontact mode, of a DPPC bilayer prepared on an annealed gold-on-glass slide. Further representative images are available in the Supporting Information (Figure S2). The images show partial coverage of the Au with DPPC. The differences in height between regions where lipids are present and where lipids are absent can be used to determine the thickness of the bilayer. Figure 3 also shows an example of a profile across a defect that was used to determine the difference in height. A series of profiles spanning a number of defects on different samples was analyzed to determine a mean difference in height of 5.4 ± 0.7 nm. (Histograms are provided in the Supporting Information, Figure S3.) This thickness is consistent with literature values for the thickness of phospholipid bilayers (e.g., ~4.8 nm for DMPC and ~5.1 nm for DMPC/cholesterol LB/LS films on Au measured with force−distance curve analysis [at a similar temperature to our experiments][49,51] or 5−6 nm for DPPC on mica, measured by analyzing defects[77]) and was subsequently used in the calculation of theoretical PM-IRRA spectra (Section 3.3).

The images were further analyzed to estimate the coverage of Au with DPPC. The areas of coated and uncoated gold were determined digitally for each image using a custom-written

https://doi.org/10.1021/acs.langmuir.1c01975
Langmuir 2021, 37, 11887−11899

MATLAB script to binarize the images and determine the proportion of pixels corresponding to heights above a given threshold. (Further details are provided in the Supporting Information, Figure S4.) The resulting coverage was found to be 83%, very close to the estimate arrived at from differential capacity results. The similarity in results from two entirely independent types of measurement is very encouraging, particularly since the capacity data, in particular, provide only an estimate of coverage. In the case of capacity data, the effects on capacity from film thickness and from average permittivity cannot be separated so a separate structural method is needed to confirm the interpretation of changes or differences in capacity. Nelson and co-workers were able to correlate DOPC film thickness on Hg with capacitance to demonstrate a phase transition between a complete monolayer and a partial bilayer on Hg.[40] In another study, Lipkowski and co-workers showed with AFM data that the thickness of DMPC bilayers was lower in the potential region of lowest capacitance and concluded that the changes in capacitance with potential were mainly related to changes in overall permittivity.[51] A similar conclusion has been drawn for DMPS bilayers, which have higher capacity but similar chain tilt angle (and therefore similar bilayer thickness) to DMPE bilayers.[62] Further, the permittivity could vary according to bilayer solvent content or presence of defects (note also that the model used above assumes no effect arises from defect size). Analysis of AFM data enables direct determination of the coverage with lipid molecules, which can aid interpretation of the capacity data, although there are very few reported comparisons of capacitance and directly determined coverage.[78]

3.3. PM-IRRAS Measurements. *3.3.1. C−H Stretching Region.* Figure 4a shows a series of representative PM-IRRA spectra, in the C−H stretching region, obtained at different applied potentials for a DPPC bilayer on Au(111). The dotted line is a calculated spectrum for a 5.4 nm layer of randomly oriented molecules on Au, with the same angle of incidence and gap thickness as for the measured spectra. In each spectrum, six bands are obtained, which may be assigned to the symmetric and asymmetric methyl group stretches (~2871 and 2960 cm^{-1}, respectively),[79−85] the symmetric and asymmetric methylene group stretches (2851 and 2920 cm^{-1}, respectively),[79−85] and two Fermi resonances (which arise from the overlap of the symmetric methylene stretching mode with overtones of the bending mode).[81,82,86] The spectra were analyzed by fitting to these six peaks, assuming a mixed Gaussian−Lorentzian line shape, as previously described.[61,62] Figure 4b illustrates the fitting of the spectrum acquired at 0 V. The band positions and full widths at half-maximum (FWHM) provide information on average chain conformation and mobility, respectively. Table 1 provides a comparison of the average values obtained from our spectra with those reported for two similar molecules, DMPC and DMPE. The band positions are between those measured for DMPC LB−LS bilayers and DMPE LB−LS bilayers and indicate that bilayers are in the gel state,[79−81,84] as expected at this temperature (the temperature of the so-called chain-melting phase transition between the gel and liquid crystalline phases is 41 °C for DPPC;[80,81] our measurements were made at 19 °C). The wavenumber is related to the average number of *gauche* conformers in hydrocarbon chains.[79,84] When a lipid assembly undergoes the chain-melting phase transition, the number of *gauche* conformers increases, and there is an increase in

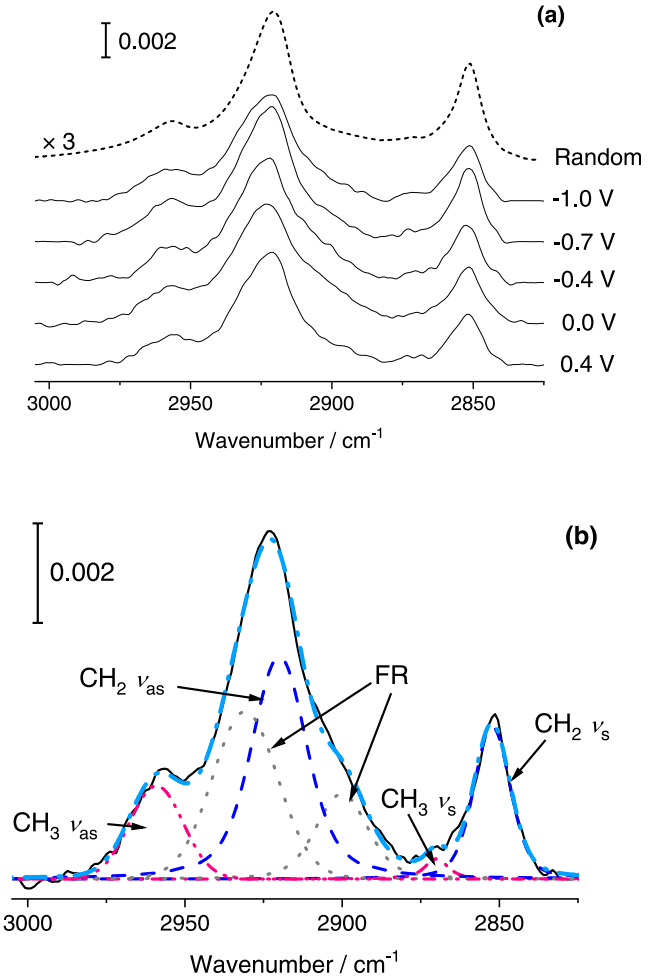

Figure 4. (a) PM-IRRA spectra for a bilayer of DPPC under potential control at selected potentials. The dotted line at the top is the simulated spectrum for a 5.4 nm thick DPPC bilayer of randomly oriented molecules. (b) Example of the deconvolution of the spectrum obtained at 0 V.

wavenumber (which is well defined for a pure lipid). Previous in situ PM-IRRAS studies on DMPC bilayers (formed from vesicle fusion or with LB−LS transfer) were carried out at ca. 20−21 °C,[35,49,50] below the DMPC phase transition temperature of 23.9 °C, and these layers were reported to be in the gel phase. An AFM study[51] explored the effect of temperature on bilayer thickness as supported bilayers become thinner in the liquid crystalline phase; a step in bilayer thickness was observed at 20−22 °C and attributed to the gel−liquid crystalline phase transition,[51] supporting the conclusion in IR studies that bilayers were in the gel phase.[35,49,50] (The slight decrease in temperature compared with other dispersions was ascribed to decoupling of, and stress within, the bilayer.[51]) Our results suggest that DPPC has fewer *gauche* conformers than DMPC, which would be expected for a longer-chain molecule at a similar temperature in a similar phase. The DPPC bilayer has more *gauche* conformers on average than DMPE bilayers investigated at the same temperature because of the tighter packing of DMPE molecules within a bilayer. (DMPE molecules are cylindrical in shape and have stronger interheadgroup interactions.) No trend in wavenumber with potential is observed for DPPC. The FWHM are close to those previously reported for DMPC,[35] which suggests that the

https://doi.org/10.1021/acs.langmuir.1c01975
Langmuir 2021, 37, 11887−11899

Table 1. Band Centers and Full Widths at Half-Maximum for Methylene Stretching Modes

	center (cm^{-1})		FWHM (cm^{-1})	
mode	$E > 0.10$ V	$E < -0.80$ V	$E > 0.10$ V	$E < -0.80$ V
$\nu_s(CH_2)$ DPPC	2851.3 ± 0.8	2851.1 ± 0.9	10.4 ± 2.6	10.1 ± 2.0
$\nu_{as}(CH_2)$ DPPC	2919.8 ± 0.6	2919.8 ± 1.0	15.9 ± 2.0	15.2 ± 1.9
$\nu_s(CH_2)$ DMPC[35]	2852.5 ± 0.5	2854.0 ± 0.3	9.5 ± 0.5	11.5 ± 0.5
$\nu_{as}(CH_2)$ DMPC[35]	2922.0 ± 0.3	2923.0 ± 0.5	16.5 ± 1.0	14.0 ± 1.0
$\nu_s(CH_2)$ DMPE[61]	2851.9 ± 0.4	2851.2 ± 0.2	11.1 ± 0.8	10.6 ± 0.7
$\nu_{as}(CH_2)$ DMPE[61]	2918.7 ± 0.1	2918.3 ± 0.1	18.8 ± 0.9	16.7 ± 0.6

degree of mobility of these two lipids on the surface is comparable.

The integrated area under a peak is related to the tilt angle of the corresponding transition dipole according to eq 3

$$\int A \, d\tilde{\nu} \propto |\boldsymbol{\mu}\cdot\boldsymbol{E}|^2 = |\mu|^2 \langle E^2 \rangle \cos^2\theta \tag{3}$$

where A is the absorbance, $\tilde{\nu}$ the wavenumber, $\boldsymbol{\mu}$ the transition dipole moment, $\boldsymbol{E}$ the electric field vector, and θ the angle between the transition dipole moment and the normal to the surface.[35,72] The peak area is also related to the amount of material present, so must be compared with the theoretical peak area for a film of randomly oriented molecules of the same thickness to calculate tilt angles, as shown in eq 4[35,72]

$$\cos^2\theta = \frac{1}{3}\frac{\int_E A \, d\tilde{\nu}}{\int_{\text{random}} A \, d\tilde{\nu}} \tag{4}$$

Figure 5a presents plots of the angles of the transition dipole moments of the symmetric and asymmetric methylene stretching modes as a function of applied potential. The chain tilt angle of the hydrocarbon chain can be evaluated from the tilt angles of the two transition dipole moments using eq 5[35,87]

$$\cos^2\theta_s + \cos^2\theta_{as} + \cos^2\theta_{chain} = 1 \tag{5}$$

where θ_s is the tilt angle of the transition dipole of the symmetric stretching mode, θ_{as} is that of the asymmetric stretching mode, and θ_{chain} is the tilt angle of the hydrocarbon chain. The directions of tilt angles are depicted in the cartoon in Figure 5b. The tilt angle is similar at both the most positive potentials (low charge density) and the most negative potentials (high charge density) at a value of 24°. As the potential is stepped in the negative direction, the tilt angle starts to rise at about 0 V (at which point the slope of the charge density-potential plot changes) and reaches a maximum at around −0.4 V, which coincides with the onset of the main electrochemical phase transition. During this phase transition, the tilt angle decreases again to its value at low charge densities. The trend does not match that observed for either DMPC or DMPE but is similar to the trend observed for asymmetric bilayers of DMPE, where one monolayer contains DMPE with per-deuterated chains (D54-DMPE) and the other monolayer contains DMPE with undeuterated chains.[88] The chains in undeuterated DMPE bilayers remain at near-constant tilt angle (17°) across the potential range. Differences in behavior between fully hydrogenous DMPE and part-deuterated DMPE bilayers were tentatively ascribed to small differences in fluidity or flexibility in the deuterated monolayer, with the packing in the deuterated monolayer affecting that in the hydrogenous monolayer.[88] The near-constant tilt angle for bilayers composed entirely of hydrogenous DMPE results from

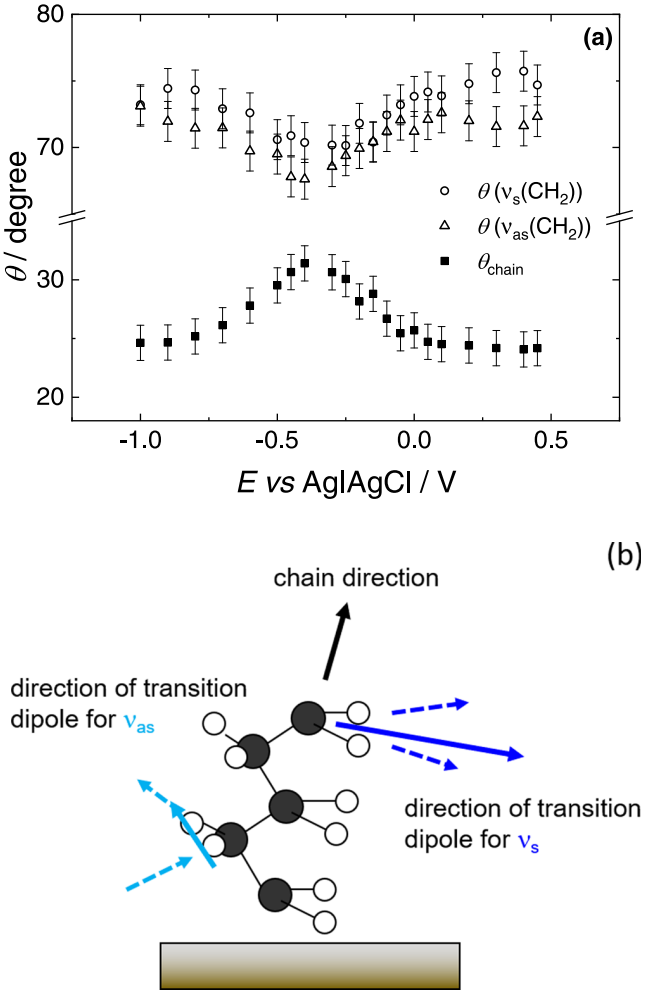

Figure 5. (a) Plot of the angles of dipole moments of symmetric (open triangles) and asymmetric (open circles) methylene stretching vibrations and of the angle of the hydrocarbon backbone (closed squares), from the surface normal, as a function of the applied potential. (b) Cartoon depicting the directions of the transition dipole moments.

tight packing of molecules, made possible by their cylindrical shape and inter-headgroup hydrogen-bonding interactions. DMPC and DPPC are both wedge-shaped molecules, with a larger headgroup footprint than DMPE. Chains are tilted more to increase the strength of dispersion interactions. DMPC and DPPC chains apparently have a similar tilt angle at positive potentials (noting that bilayers were deposited at the same area per molecule, despite different surface pressure). DMPC chains also increase in tilt angle over a potential range ~ −0.05 to ~ −0.45 V but to a lesser degree than DPPC (only ~3°), but the tilt angle decreases through the electrochemical phase

https://doi.org/10.1021/acs.langmuir.1c01975
Langmuir 2021, 37, 11887−11899

transition to a value of 17° at negative potentials. The small rise in the tilt angle just positive of this transition was attributed to electrostriction of the film, and it is possible that electrostriction also explains the increase in angle for DPPC. However, it is not clear why the extent is greater because the surface pressure for the DPPC deposition was slightly higher than for DMPC, the compressibility moduli from our DMPC[67] and DPPC isotherms at 45 Å^2 are very similar (at 18 °C—note that the isotherms of DMPC layers in ref 35 were measured at 22 °C), and, for supported bilayers, the spectra for DPPC and DMPC chains indicated similar mobility of the molecules. It is possible that the larger increase is related to a change in conformation around the linkage to the glycerol moiety (vide infra).

The main phase transition was reported for DMPC and DMPC/cholesterol mixtures to result from the movement of solvent molecules through the film to the surface in response to the increasing electric field.[36,49,63] The lipid bilayer was directly adsorbed at the surface positive of the transition and adsorbed on a thin cushion of electrolyte negative of the transition, which means a change in the environment for the surface-facing half of the bilayer. This change in the environment was suggested to be responsible for the observed change in the tilt angle of hydrocarbon chains as headgroups adopted a staggered, zigzag arrangement on the aqueous cushion.[36,49,63] Subsequent in situ AFM experiments demonstrated a change in bilayer morphology.[51] The structural changes arise from the distribution of the electrolyte because the same structure for the directly adsorbed bilayers was observed both for reconstructed surfaces and for surfaces where the reconstruction had been lifted.[51] If the phase transition observed for DPPC can be interpreted in the same way as for DMPC, as resulting from the formation of an aqueous layer between lipid and surface, then the final state of the bilayer on the electrolyte cushion at the negative potential limit has a similar structure to that in the positive potential range, rather than the different structure observed for DMPC. The most likely explanation is that DPPC headgroups do not adopt the same zigzag arrangement proposed for DMPC headgroups at negative charge density, perhaps because dispersion forces between longer chains are stronger and closer packing of headgroups is unnecessary to allow closer proximity of tails. Watkins et al. reported tilt angles for chains of DPPC bilayers on quartz substrates (also transferred by LB−LS at 45 mN m^{-1}): 27.3° was obtained from X-ray reflectivity measurements and 26.8° was obtained from in-plane grazing incidence X-ray diffraction (GIXD) measurements.[16] Our values are within the experimental error of values reported for bilayers on quartz. Those bilayers were separated from quartz by a thin water layer (∼4.2 Å)[16] so it is possible that the presence or absence of the water layer does not alter significantly the structure observed on Au for DPPC.

Methylene groups also have a bending (scissoring) mode at ∼1468 cm^{-1}. A single peak has been reported for chains packed in a hexagonal or triclinic arrangement and a split peak for chains packed in an orthorhombic structure, where the rotational orientation of chains is restricted such that the bisectors of the CH_2 groups of nearest neighbor chains point in different directions.[89] GIXD shows that chains in DPPC monolayers on water are packed in a similar in-plane geometric arrangement to the orthorhombic structure but have rotational freedom about the chain axis.[90] In this case, the packing may be termed distorted hexagonal.[89,90] This distorted hexagonal structure should result in a more random rotational orientation of the methylene groups, so the chains would be expected to produce one peak corresponding to IR bending mode vibrations, as the rotational orientations of nearest neighbor chains are equivalent. In one study of DPPC multilayers, splitting of the scissoring mode was reported at temperatures below 10 °C,[89] whereas in a later study by the same authors, some evidence of splitting was detected at higher temperatures.[81] Le Bihan and Pezolet observed overlapping bands attributed to triclinic (1471 cm^{-1}) and hexagonal (1467 cm^{-1}) structures, the ratio of which was dependent on temperature and on prior incubation of the samples at low temperature. At ∼20 °C, the spectra indicated mostly hexagonal packing.[91] Our spectra show one peak (Supporting Information, Figure S5), which suggests at least some rotational disorder in DPPC chains. GIXD has also been utilized to investigate the structure of DPPC on quartz in detail, comparing structures formed with LB/LS deposition at several surface pressures with those of monolayers at various surface pressures and bilayers formed via vesicle deposition.[90] Although the area per molecule was reported to change little on LB−LS deposition, the data could only be fitted if some restriction to rotation around the chain axis was included in the model structure. This restriction was accounted for by strong inter-leaflet coupling. In this case, a range of rotational tilt angles was determined.[90] If our bilayers supported on Au have a similar structure to those supported on quartz and are well organized but have some degree of rotational freedom, one peak for the methylene bending mode may be expected in our spectra. It is worth noting that the tilt angles for the dipole moments of our asymmetric and symmetric methylene stretching modes are slightly different, more so than for DMPC, which might suggest some restriction to rotation around the chain axis, as was seen on quartz, although the difference is small and similar to the expected error (∼3°). The difference is, however, consistent across the potential range until −1.0 V.

3.3.2. Headgroup Vibrations. The choline group has vibrations in the range 1450−1500 cm^{-1}, which overlap with the bending mode of CH_2 groups in hydrocarbon chains at ∼1468 cm^{-1}. The spectra in this region were rather noisy, but bands could be fitted at ∼1480 and at 1490 cm^{-1}, corresponding to the $\delta_{as}(NMe_3^+)$ vibrations, and at 1457 cm^{-1}, corresponding to the chain asymmetric methyl deformations.[35,92] Background subtraction and fitting of the data in this region is prone to significant error because of the strong background signal so the data were not analyzed quantitatively. However, there was a similar trend in the intensity of the ∼1480 cm^{-1} vibration to that reported for DMPC, suggesting a small change in orientation of the choline group during the electrochemical phase transition. Vibrations corresponding to C−N stretching of choline groups can also be expected in the low wavenumber region. Spectra acquired in that region are shown in the Supporting Information, Figure S6. The spectra can be fitted with peaks at 970, 952, and 931 cm^{-1}. Following Zawisza et al. for DMPC,[35,92] the first two correspond to asymmetric stretching and the last to a symmetric stretch.[92] Although the lower wavenumber counterpart of the symmetric stretch cannot be observed in our spectra (expected at ∼860 cm^{-1}, close to the cutoff) and cannot be used to aid assignment, the wavenumber of the observed peak would suggest a *trans* conformation for the choline group rather than the *gauche* conformation reported for DMPC[35] or DOPC[56] bilayers (the latter formed from vesicles), as we

https://doi.org/10.1021/acs.langmuir.1c01975
Langmuir 2021, 37, 11887−11899

observed in our transmission spectra of DPPC vesicles. A small increase in the intensity of the 931 cm^{-1} peak occurs negative of the main phase transition, which may correlate with the change in orientation of the deformation dipole moment. However, errors in baseline subtraction in this spectral region mean that it is difficult to calculate tilt angles with confidence. Apparently, the LB−LS deposition of DPPC does not result in a change in headgroup conformation, unlike for DMPC.

Figure 6 shows spectra acquired in the region where phosphate vibrations are observed. In Figure 6a, the phosphate

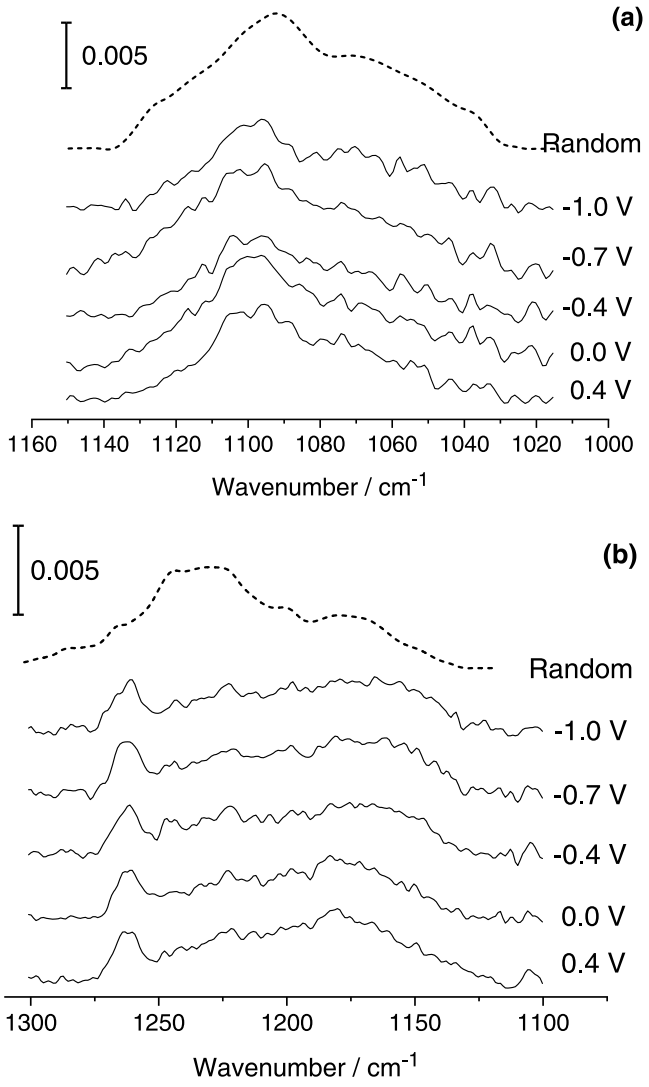

Figure 6. Spectra obtained in the phosphate stretching mode region for Au(111) with an LB−LS bilayer of DPPC in a 0.1 M NaF electrolyte at selected applied potentials. The dotted lines are the simulated spectra calculated for a 5.4 nm thick DPPC bilayer of randomly oriented molecules with the same cell setup. (a) Symmetric stretching mode region. (b) Asymmetric stretching mode region.

PO_2^- symmetric stretch is observed at ∼1098.5 cm^{-1}, overlapping with C−O−P vibrations at 1056, 1073, and 1119 cm^{-1}. The wavenumber of the symmetric PO_2^- O−P−O stretch is invariant with potential, and its value is indicative of unsolvated phosphate groups; the wavenumber for this mode in the spectra obtained from vesicles is 1089.9 cm^{-1}, similar to the value reported for DMPC.[35]

The spectra in Figure 6b include a band related to the ester group (discussed further below) at ∼1170−1180 cm^{-1}, the asymmetric PO_2^- O−P−O stretching mode at ∼1230 cm^{-1}, and a series of peaks corresponding to the CH_2 wagging mode progression.[81,93] One of these is clearly resolved at 1262 cm^{-1} and the others, expected at 1200, 1220, and 1245 cm^{-1}, are combined with the phosphate asymmetric stretching mode but can be discerned as "bumps" on a broad envelope. The wagging mode vibrations are more prominent in the bilayer than in the theoretical spectrum because in the bilayer their transition dipole moments are aligned roughly along the direction of the chain axis,[92] whereas the direction of the phosphate mode transition dipole would be expected to be closer to parallel to the surface. The asymmetric PO_2^- stretching mode for the bilayer is located at around 1230 cm^{-1}, which is similar to its position in the spectra of vesicles and indicative of a relatively solvated phosphate group, not dissimilar to the case of adsorbed DMPC.[35] The origin of the difference in the degree of solvation implied by the symmetric and asymmetric stretching modes is unclear because the spectra were acquired in the same measurements. It is possible that the picture is more complex: similar band position and shape for the symmetric stretching mode were also found for DMPS bilayers that had a relatively high solvent content.[62] Although the overlap of the asymmetric mode with the wagging mode progression makes analysis of this band difficult, the overall distribution of intensity within the peak would imply a reasonable level of solvation, similar to that reported for DMPC.[35]

A tilt angle can be estimated for the CO−P−OC backbone from O−P−O stretches, in a similar fashion to the calculation for hydrocarbon chains (eq 5).[35] The tilt angles obtained for the symmetric stretching mode showed a small change as the potential was made more negative, from approximately 68° to 71° (Figure S7). The tilt angles for the asymmetric stretch cannot be calculated with confidence because of the overlap with the wagging modes, but our best estimate suggests an average tilt angle for this mode of around 76−77°. The resulting tilt angles for the CO−P−OC backbone are presented in the Supporting Information (Figure S7) and range from around 27° at positive potentials to around 24° at negative potentials, within the error of the values reported for DMPC.[35] A maximum value for this tilt angle (obtained by assuming the peak intensity of all but the 1180 and 1262 cm^{-1} bands arise entirely from phosphate modes) would be around 30°, similar to the tilt angle for deuterated DMPE bilayers at positive potentials.[61] The resulting trend in the tilt angle with potential is weak and within the likely margin of error (∼5°), but trends reported for other phospholipids are also very small.[35,61,62]

The band at ∼1170 cm^{-1} in Figure 6b is assigned to a vibration of ester carbonyl groups.[35,92] The ester groups typically give rise to two peaks in IR spectra, one at around 1730 cm^{-1}, which has largely C═O character, and one at around 1170 cm^{-1}, which is dominated by the C−O stretch of the acylated oxygen atom (C−O−C).[92] Both are sensitive to the extent of hydrogen bonding in which the ester groups participate.[92] The latter is also sensitive to the conformation of this part of the molecule.[92] Figure 7 shows the C−O−C vibration band center as a function of applied potential. As the potential is made more negative, the wavenumber decreases from 1177 to 1168 cm^{-1}, which indicates either a change in the solvation of the ester groups or a change in the dihedral

https://doi.org/10.1021/acs.langmuir.1c01975
Langmuir 2021, 37, 11887−11899

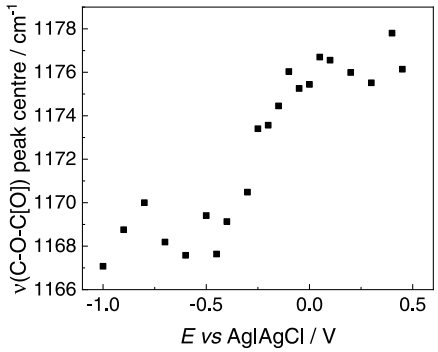

Figure 7. Plot of the C−O peak position as a function of potential.

angle.[92] DPPC has been reported to consist of a "nonuniform" conformation of headgroups, with a mixture of dihedral angles.[92] A planar conformation with a dihedral angle of 180° is associated with a peak position of 1180 cm^{-1} and a lower wavenumber is associated with a nonplanar conformation of the ester group. The plot in Figure 7 shows that the angle is close to planar at positive potentials, where DPPC is adsorbed, and nonplanar at negative potentials, where it is lifted from the electrode surface, the opposite trend from DMPC bilayers.

3.3.3. C═O Stretching Region. A series of spectra acquired for different potentials in the carbonyl stretching region is presented in Figure 8a. The dotted line represents the simulated spectrum of a film of randomly oriented molecules under the same experimental conditions. An intense band of asymmetric shape is observed in all of the spectra. This band may be fitted as two peaks centered at 1728 and 1740 cm^{-1}. The former corresponds to C═O stretching of ester groups involved in hydrogen bonding to water (strongly solvated), and the latter corresponds to C═O stretching of ester groups not involved in hydrogen bonding (poorly solvated).[35,84,94,95] The shape of the band alters with potential and the effect can be interpreted by considering the proportion of the total band area made up of either the "solvated" or "unsolvated" carbonyl stretching mode, as described previously.[61,62] Figure 8b shows a plot of the percentage of the band area corresponding to "unsolvated" ester groups, overlaid on a plot of the change in the hydrocarbon chain tilt angle. A clear change in the degree of hydration of the bilayer is observed: the bilayer is relatively hydrated at low charge densities compared with at higher charge densities and the change is concomitant with the change in the hydrocarbon chain tilt angle. DMPC carbonyl groups are also less solvated at negative potentials when water has left the bilayer and formed a cushion between the Au and the bilayer.[35] In the case of DPPC, a weak trend toward lower wavenumber of the asymmetric phosphate stretching mode implies greater solvation of phosphate groups as carbonyl groups become less solvated, which suggests a movement of water from the ester groups out of the bilayer. DMPC, by contrast, was shown to have less solvated phosphate groups in the desorbed layer, but this may be explained by the proposed zigzag arrangement of headgroups,[35] which may lead to squeezing out of some water molecules from the headgroup region. Since the chain tilt angles indicate that DPPC headgroups probably do not adopt a zigzag arrangement and there is little change in phosphate orientation, water may not be squeezed out.

The onset of the change from planar to nonplanar conformation coincides with the decrease in solvation of

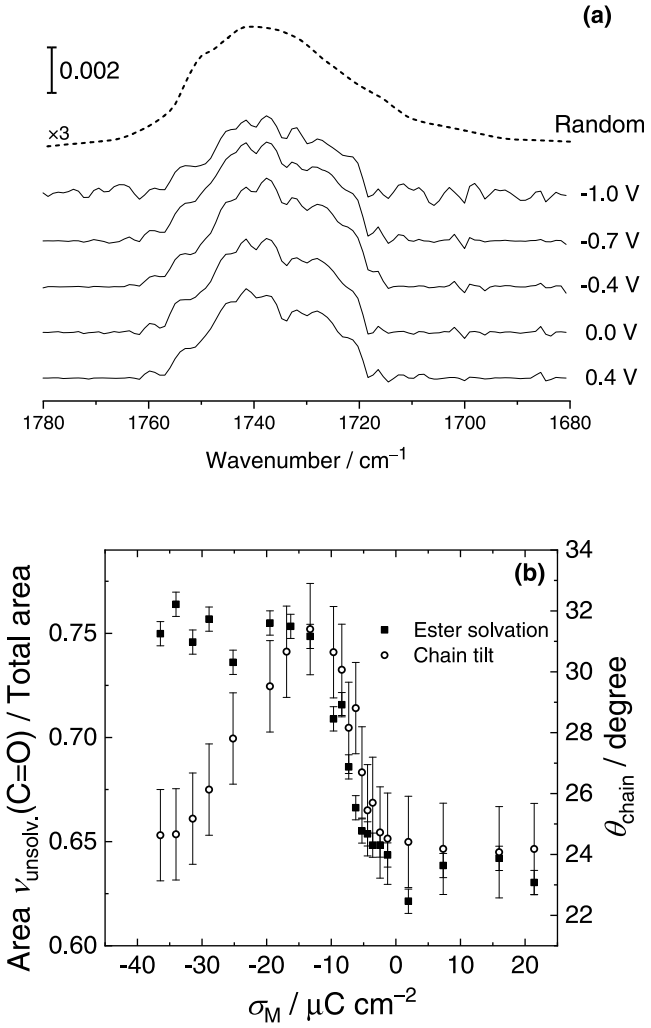

Figure 8. (a) Spectra in the C═O stretching region for a DPPC bilayer on Au(111) in 0.1 M NaF at selected potentials. The dotted line is the simulated spectrum for a 5.4 nm thick DPPC bilayer of randomly oriented molecules. (b) Plot of the proportion of the C═O stretching mode band corresponding to "unsolvated" carbonyl groups (left axis) and the chain tilt of that bilayer (right axis) against surface charge.

carbonyl groups and the increase in tilt angle of hydrocarbon chains as the potential is made more negative (Figure S8). Hence, it is possible that the increase in the chain tilt angle results from the change in conformation around the ester group, which may result from the egress of water from the bilayer. As the potential becomes more negative and the water layer forms between the lipid and substrate, the carbonyl groups retain their new conformation and solvation state, but the chains (or one of the chains) may then reorient by forming an additional *gauche* conformer near the base of the chain, to return to the original tilt angle. If this is the case, it would imply that the structure of the bilayer on Au is driven by chain−chain interactions, which was also suggested to be a major factor for DPPC bilayers supported on quartz.[90]

4. CONCLUSIONS

The effect of an applied electric field on the behavior of DPPC bilayers supported on Au(111) has been studied with a combination of electrochemical methods, AFM and in situ PM-IRRAS. The coverage of DPPC on Au substrates

https://doi.org/10.1021/acs.langmuir.1c01975
Langmuir 2021, 37, 11887−11899

estimated from differential capacitance measurements was found to match very well that determined from AFM images, at ~83%. The bilayers are slightly thicker than those reported for DMPC bilayers.[49,51] The electrochemical response of DPPC bilayers appears similar to that reported for other phospholipids, but the PM-IRRAS data show differences in the bilayer structure on either side of the electrochemical phase transition.

At small, positive charge densities, the hydrocarbon chains adopt a similar tilt angle to those of DMPC and also undergo compression as the surface charge is made negative, resulting in an increase in the chain tilt angle from the surface normal. However, while DMPC molecules adopt a zigzag arrangement of headgroups, with chains less tilted, at the most negative charge densities, DPPC chains return to the same tilt angle as they have at positive potentials, and there is only very little change in headgroup orientation. The conformation of the headgroups of DPPC and DMPC differ, with DPPC in bilayers similar to DPPC in aqueous dispersions. The changes in conformation about the C−O−C bond of the acyl chain linkage to the glycerol backbone also differ: DPPC molecules adopt a planar conformation at positive charge densities and an off-planar conformation at negative charge densities, which may be caused by the change in solvation of the carbonyl groups and which permits chains to adopt a preferred tilt angle at negative charge densities. The change in solvation of the carbonyl groups occurs as the surface charge density is made more negative and this, along with the shapes of the capacitance-potential and charge-potential curves, suggests that the solvent leaves the bilayer to form a cushion between the bilayer and surface, as was reported for DMPC bilayers. The fact that headgroup orientation changes little and chain tilt is the same in both states implies molecules adjust their conformation to maintain a preferred chain orientation rather than reorienting their headgroups. This leads us to conclude that the structure of the DPPC bilayer is driven primarily by chain−chain interactions and possibly coupling between the two monolayers, as was observed for bilayers on quartz.[90] DPPC is less influenced by the substrate than DMPC because of stronger dispersion forces between longer chains. To comprehend fully the nature of a biological cell membrane, it is necessary to obtain information on a range of systems (including mixtures) so that we may better understand the interplay between various intermolecular interactions that may be involved in determining the structure and behavior. The results from this study demonstrate how very subtle variations in molecule structure may have a significant impact on the structure and behavior of the ensemble of molecules, including in their response to a static electric field of comparable magnitude to those found in nature. This may in turn affect membrane breakdown at high fields and local membrane structure around proteins, potentially affecting their function.

■ ASSOCIATED CONTENT

Supporting Information

The Supporting Information is available free of charge at https://pubs.acs.org/doi/10.1021/acs.langmuir.1c01975.

Surface pressure-area isotherm, additional AFM images and details of their analysis, and additional IR spectra and analysis (PDF)

■ AUTHOR INFORMATION

Corresponding Author

Sarah L. Horswell − *School of Chemistry, University of Birmingham, Birmingham B15 2TT, U.K.;* orcid.org/0000-0001-9079-8551; Phone: +44 (0)121 414 7474; Email: s.l.horswell@bham.ac.uk

Authors

Philip N. Jemmett − *School of Chemistry, University of Birmingham, Birmingham B15 2TT, U.K.*

David C. Milan − *Department of Chemistry, University of Liverpool, Liverpool L69 7ZD, U.K.*

Richard J. Nichols − *Department of Chemistry, University of Liverpool, Liverpool L69 7ZD, U.K.*

Liam R. Cox − *School of Chemistry, University of Birmingham, Birmingham B15 2TT, U.K.;* orcid.org/0000-0001-7018-3904

Complete contact information is available at: https://pubs.acs.org/10.1021/acs.langmuir.1c01975

Notes

The authors declare no competing financial interest.

■ ACKNOWLEDGMENTS

This work was supported by the BBSRC-funded Midlands Integrative Biosciences Training Partnership Centre for Doctoral Training (grant number BB/J014532/1). The authors are indebted to Prof. V. Zamlynny and Prof. J. Lipkowski for kindly allowing the authors to use the Fresnel software and to Dr. A. L. N. Pinheiro for help with the data acquisition software. The technical support of A. Rothin, S. Williams, and S. G. Arkless is gratefully acknowledged. Data created during this research are openly available from the UBIRA eData repository at https://doi.org/10.25500/edata.bham.00000718.

■ REFERENCES

(1) van Meer, G.; de Kroon, I. P. M. Lipid Map of the Mammalian Cell. *J. Cell Sci.* **2011**, *124*, 5−8.

(2) Skipski, V. P.; Barclay, M.; Archibald, F. M.; Terebus-Kekish, O.; Reichman, E. S.; Good, J. J. Lipid Composition of Rat Liver Cell Membranes. *Life Sci.* **1965**, *4*, 1673−1680.

(3) Spector, A. A.; Yorek, M. A. Membrane Lipid Composition and Cellular Function. *J. Lipid Res.* **1985**, *26*, 1015−1035.

(4) Stübiger, G.; Pittenauer, E.; Belgacem, O.; Rehulka, P.; Widhalm, K.; Allnaier, G. Analysis of Human Plasma Lipids and Soybean Lecithin by means of High-Performance Thin-Layer Chromatography and Matrix-Assisted Laser Desorption/Ionization Mass Spectrometry. *Rapid Commun. Mass Spectrom.* **2009**, *23*, 2711−2723.

(5) Wijesooriya, C.; Budai, M.; Budai, L.; Szilasi, M.; Petrikovics, I. Optimization of Liposomal Encapsulation for Ceftazidime for Developing a Potential Eye Drop Formulation. *J. Basic Clin. Pharm.* **2013**, *4*, 73−75.

(6) Mishra, G. P.; Bagui, M.; Tamboli, V.; Mitra, A. K. Recent Applications of Liposomes in Ophthalmic Drug Delivery. *J. Drug Delivery* **2011**, No. 863734.

(7) Natarajan, J. V.; Chattopadhyay, S.; Ang, M.; Darwitan, A.; Foo, S.; Zhen, M.; Koo, M.; Wong, T. T.; Venkatraman, S. S. Sustained Release of an Anti-Glaucoma Drug: Demonstration of Efficacy of a Liposomal Formulation in the Rabbit Eye. *PLoS One* **2011**, *6*, No. e24513.

(8) Yu, S.-H.; Possmayer, F. Comparative Studies on the Biophysical Activities of the Low-Molecular-Weight Hydrophobic Proteins Purified from Bovine Pulmonary Surfactant. *Biochim. Biophys. Acta, Lipids Lipid Metab.* **1988**, *961*, 337−350.

(9) Yu, S-H.; Possmayer, F. Effect of Pulmonary Surfactant Protein B (SP-B) and Calcium on Phospholipid Adsorption and Squeeze-out of Phosphatidylglycerol from Binary Phospholipid Monolayers Containing Dipalmitoylphosphatidylcholine. *Biochim. Biophys. Acta, Lipids Lipid Metab.* **1992**, *1126*, 26−34.
(10) Hasanovic, A.; Hollick, C.; Fischinger, K.; Valenta, C. Improvement in Physicochemical Parameters of DPPC Liposomes and Increase in Skin Permeation of Aciclovir and Minoxidil by the Addition of Cationic Polymers. *Eur. J. Pharm. Biopharm.* **2010**, *75*, 148−153.
(11) Hasanovic, A.; Hoeller, S.; Valenta, C. Analysis of Skin Penetration of Phytosphingosine by Fluorescence Detection and Influence of the Thermotropic Behaviour of DPPC Liposomes. *Int. J. Pharm.* **2010**, *383*, 14−17.
(12) Nikoleli, G.-P.; Siontorou, C. G.; Nikolelis, D. P.; Bratakou, S.; Karapetis, S.; Tzamtzis, N. Biosensors Based on Lipid Modified Graphene Microelectrodes. *C* **2017**, *3*, No. 9.
(13) Peetla, C.; Stine, A.; Labhasetwar, V. Biophysical Interactions with Model Lipid Membranes: Applications in Drug Discovery and Drug Delivery. *Mol. Pharmaceutics* **2009**, *6*, 1264−1276.
(14) Sebinelli, H. G.; Borin, I. A.; Ciancaglini, P.; Bolean, M. Topographical and Mechanical Properties of Liposome Surfaces Harboring Na,K-ATPase by means of Atomic Force Microscopy. *Soft Matter* **2019**, *15*, 2737−2745.
(15) Nunes, C.; Brezesinksi, G.; Lopes, D.; Lima, J. L. F. C.; Reis, S.; Lucio, M. Lipid-Drug Interaction: Biophysical Effects of Tolmetin on Membrane Mimetic Systems of Different Dimensionality. *J. Phys. Chem. B* **2011**, *115*, 12615−12625.
(16) Watkins, E. B.; Miller, C. E.; Mulder, D. J.; Kuhl, T. L.; Majewski, J. Structure and Orientational Texture of Self-Organizing Lipid Bilayers. *Phys. Rev. Lett.* **2009**, *102*, No. 238101.
(17) Nyholm, T.; Nylund, M.; Söderholm, A.; Slotte, J. P. Properties of Palmitoyl Phosphatidylcholine, Sphingomyelin, and Dihydrosphingomyelin Bilayer Membranes as Reported by Different Fluorescent Reporter Molecules. *Biophys. J.* **2003**, *84*, 987−997.
(18) Charitat, T.; Bellet-Amalric, E.; Fragneto, G.; Graner, F. Adsorbed and Free Lipid Bilayers at the Solid-Liquid Interface. *Eur. Phys. J. B* **1999**, *8*, 583−593.
(19) Sarkis, J.; Vié, V. Biomimetic Models to Investigate Membrane Biophysics Affecting Lipid−Protein Interaction. *Front. Bioeng. Biotechnol.* **2020**, *8*, No. 270.
(20) Sánchez, S. A.; Tricerri, M. A.; Ossato, G.; Gratton, E. Lipid Packing Determines Protein-Membrane Interactions: Challenges for Apolipoprotein A−I and High Density Lipoproteins. *Biochim. Biophys. Acta, Biomembr.* **2010**, *1798*, 1399−1408.
(21) Contreras, F-X.; Ernst, A. M.; Wieland, F.; Brügger, B. Specificity of Intramembrane Protein− Lipid Interactions. *Cold Spring Harbor Perspect. Biol.* **2011**, *3*, No. a004705.
(22) Corradi, V.; Sejdiu, B. I.; Mesa-Galloso, H.; Abdizadeh, H.; Noskov, S. Y.; Marrink, S. J.; Tieleman, D. P. Emerging Diversity in Lipid−Protein Interactions. *Chem. Rev.* **2019**, *119*, 5775−5848.
(23) Luchini, A.; Vitiello, G. Mimicking the Mammalian Plasma Membrane: An Overview of Lipid Membrane Models for Biophysical Studies. *Biomimetics* **2021**, *6*, No. 3.
(24) Munusamy, S.; Conde, R.; Bertrand, B.; Munoz-Garay, C. Biophysical Approaches for Exploring Lipopeptide-Lipid Interactions. *Biochimie* **2020**, *170*, 173−202.
(25) Greenwood, A. I.; Tristram-Nagle, S.; Nagle, J. F. Partial Molecular Volumes of Lipids and Cholesterol. *Chem. Phys. Lipids* **2006**, *143*, 1−10.
(26) Biltonen, R. L.; Lichtenberg, D. The Use of Differential Scanning Calorimetry as a Tool to Characterize Liposome Preparations. *Chem. Phys. Lipids* **1993**, *64*, 129−142.
(27) Meyer, H. W.; Semmler, K.; Rettig, W.; Pohle, W.; Ulrich, A. S.; Grage, S.; Selle, C.; Quinn, P. J. Hydration of DMPC and DPPC at 4 °C Produces a Novel Subgel Phase with Convex−Concave Bilayer Curvatures. *Chem. Phys. Lipids* **2000**, *105*, 149−166.
(28) Helm, C. A.; Möhwald, H.; Kjær, K.; Als-Nielsen, J. Phospholipid Monolayer Density Distribution Perpendicular to the Water Surface. A Synchrotron X-ray Reflectivity Study. *Europhys. Lett.* **1987**, *4*, 697−703.
(29) Kienle, D. F.; de Souza, J. V.; Watkins, E. B.; Kuhl, T. L. Thickness and Refractive Index of DPPC and DPPE Monolayers by Multiple-Beam Interferometry. *Anal. Bioanal. Chem.* **2014**, *406*, 4725−4733.
(30) Nagle, J. F.; Tristram-Nagle, S. Structure of Lipid Bilayers. *Biochim. Biophys. Acta, Rev. Biomembr.* **2000**, *1469*, 159−195.
(31) Kučerka, N.; Nagle, J. F.; Sachs, J. N.; Feller, S. E.; Pencer, J.; Jackson, A.; Katsaras, J. Lipid Bilayer Structure Determined by the Simultaneous Analysis of Neutron and X-ray Scattering Data. *Biophys. J.* **2008**, *95*, 2356−2367.
(32) Wong, P. T. T.; Mantsch, H. H. High-Pressure Infrared Spectroscopic Evidence of Water Binding Sites in 1,2-Diacyl Phospholipids. *Chem. Phys. Lipids* **1988**, *46*, 213−224.
(33) Alberts, B.; Johnson, A.; Lewis, J.; Raff, M.; Roberts, K.; Walter, P. *Molecular Biology of the Cell*, 4th ed.; Taylor and Francis: London, 2002; Chapter 10.
(34) Tsong, T. Y.; Astumian, R. D. Electroconformational Coupling: How Membrane-Bound ATPase Transduces Energy From Dynamic Electric Fields. *Annu. Rev. Physiol.* **1988**, *50*, 273−290.
(35) Zawisza, I.; Bin, X.; Lipkowski, J. Potential-Driven Structural Changes in Langmuir-Blodgett DMPC Bilayers Determined by In Situ Spectroelectrochemical PM IRRAS. *Langmuir* **2007**, *23*, 5180−5194.
(36) Burgess, I.; Li, M.; Horswell, S. L.; Szymanski, G.; Lipkowski, J.; Majewski, J.; Satija, S. Electric Field—Driven Transformations of a Supported Model Biological Membrane-An Electrochemical and Neutron Reflectivity Study. *Biophys. J.* **2004**, *86*, 1763−1776.
(37) Nelson, A.; Benton, A. Phospholipid Monolayers at the Mercury-Water Interface. *J. Electroanal. Chem.* **1986**, *202*, 253−270.
(38) Bizzotto, D.; Nelson, A. Continuing electrochemical studies of phospholipid monolayers of dioleoyl phosphatidyl choline at the mercury−electrolyte interface. *Langmuir* **1998**, *14*, 6269−6273.
(39) Whitehouse, C.; O'Flanagan, R.; Lindholm-Sethson, B.; Movaghar, B.; Nelson, A. Application of Electrochemical Impedance Spectroscopy to the Study of Dioleoyl Phosphatidylcholine Monolayers on Mercury. *Langmuir* **2004**, *20*, 136−144.
(40) Rashid, A.; Vakurov, A.; Nelson, A. Phospholipid Bilayers at the Mercury (Hg)/Water Interface. *Electrochim. Acta* **2018**, *281*, 152−161.
(41) Leermakers, F. A. M.; Nelson, A. Substrate-induced structural changes in electrode-adsorbed lipid layers—A self-consistent field theory. *J. Electroanal. Chem. Interfacial Electrochem.* **1990**, *278*, 53−72.
(42) Brukhno, A. V.; Akinshina, A.; Coldrick, Z.; Nelson, A.; Auer, S. Phase phenomena in supported lipid films under varying electric potential. *Soft Matter* **2011**, *7*, 1006−1017.
(43) Bizzotto, D.; Yang, Y.; Shepherd, J.; Stoodley, R.; Agak, J.; Stauffer, V.; Lathuilliere, M.; Akhtar, A. S.; Chung, E. Electrochemical and spectroelectrochemical characterization of lipid organization in an electric field. *J. Electroanal. Chem.* **2004**, *574*, 167−184.
(44) Becucci, L.; Moncelli, M. R.; Herrero, R.; Guidelli, R. Dipole Potentials of Monolayers of Phosphatidylcholine, Phosphatidylserine and Phosphatidic Acid on Mercury. *Langmuir* **2000**, *16*, 7694−7700.
(45) Moncelli, M. R.; Becucci, L.; Buoninsegni, F. T.; Guidelli, R. Surface Dipole Potential at the Interface Between Water and Self-Assembled Monolayers of Phosphatidylserine and Phosphatidic Acid. *Biophys. J.* **1998**, *74*, 2388−2397.
(46) Becucci, L.; Martinuzzi, S.; Monetti, E.; Mercatelli, R.; Quercioli, F.; Battistel, D.; Guidelli, R. Electrochemical Impedance Spectroscopy and Fluorescence Lifetime Imaging of Lipid Mixtures Self-Assembled on Mercury. *Soft Matter* **2010**, *6*, 2733−2741.
(47) Rueda, M.; Navarro, I.; Prieto, F.; Nelson, A.; et al. Impedance Measurements with Phospholipid-Coated Mercury Electrodes. *J. Electroanal. Chem.* **1998**, *454*, 155−160.
(48) Rueda, M.; Navarro, I.; Prado, C.; Silva, C. Impedance Study of Tl+ Reduction at Gramicidin-Modified Dioleoylphosphatidylcholine-Coated Mercury Electrodes: Influence of Gramicidin Concentration

and the Nature of the Supporting Electrolyte. *J. Electrochem. Soc.* **2001**, *148*, E139−E147.
(49) Lipkowski, J. Building Biomimetic Membrane at a Gold Electrode Surface. *Phys. Chem. Chem. Phys.* **2010**, *12*, 13874−13887.
(50) Bin, X.; Zawisza, I.; Goddard, J. D.; Lipkowski, J. Electrochemical and PM-IRRAS studies of the effect of the static electric field on the structure of the DMPC bilayer supported at a Au(111) electrode surface. *Langmuir* **2005**, *21*, 330−347.
(51) Li, M.; Chen, M.; Sheepwash, E.; Brosseau, C. L.; Li, H.; Pettinger, B.; Gruler, H.; Lipkowski, J. AFM Studies of Solid-Supported Lipid Bilayers Formed at a Au(111) Electrode Surface Using Vesicle Fusion and a Combination of Langmuir-Blodgett and Langmuir-Schaefer Techniques. *Langmuir* **2008**, *24*, 10313−10323.
(52) Abbasi, F.; Leitch, J. J.; Su, Z. F.; Szymanski, G.; Lipkowski, J. Direct Visualization of Alamethicin Ion Pores Formed in a Floating Phospholipid Membrane Supported on a Gold Electrode Surface. *Electrochim. Acta* **2018**, *267*, 195−205.
(53) Dziubak, D.; Strzelak, K.; Sek, S. Electrochemical Properties of Lipid Membranes Self-Assembled From Bicelles. *Membranes* **2021**, *11*, No. 11.
(54) Sek, S.; Xu, S.; Chen, M.; Szymanski, G.; Lipkowski, J. STM Studies of Fusion of Cholesterol Suspensions and Mixed 1,2-Dimyristoyl-sn-glycero-3-phosphocholine (DMPC)/Cholesterol Vesicles onto a Au(111) Electrode Surface. *J. Am. Chem. Soc.* **2008**, *130*, 5736−5743.
(55) Sek, S.; Laredo, T.; Dutcher, J. R.; Lipkowski, J. Molecular Resolution Imaging of an Antibiotic Peptide in a Lipid Matrix. *J. Am. Chem. Soc.* **2009**, *131*, 6439−6444.
(56) Zawisza, I.; Lachenwitzer, A.; Zamlynny, V.; Horswell, S. L.; Goddard, J. D.; Lipkowski, J. Electrochemical and Photon Polarization Modulation Infrared Reflection Absorption Spectroscopy Study of the Electric Field Driven Transformations of a Phospholipid Bilayer Supported at a Gold Electrode Surface. *Biophys. J.* **2003**, *85*, 4055−4075.
(57) Uchida, T.; Osawa, M.; Lipkowski, J. SEIRAS Studies of Water Structure at the Gold Electrode Surface in the Presence of Supported Lipid Bilayer. *J. Electroanal. Chem.* **2014**, *716*, 112−119.
(58) Su, Z. F.; Shodiev, M.; Leitch, J. J.; Abbasi, F.; Lipkowski, J. Role of Transmembrane Potential and Defects on the Permeabilization of Lipid Bilayers by Alamethicin, an Ion-Channel-Forming Peptide. *Langmuir* **2018**, *34*, 6249−6260.
(59) Brand, I.; Matyszewska, D.; Koch, K.-W. Binding of a Myristoylated Protein to the Lipid Membrane Influenced by Interactions with the Polar Head Group Region. *Langmuir* **2018**, *34*, 14022−14032.
(60) Brand, I.; Koch, K. W. Impact of the Protein Myristoylation on the Structure of a Model Cell Membrane in a Protein Bound State. *Bioelectrochemistry* **2018**, *124*, 13−21.
(61) Madrid, E.; Horswell, S. L. Effect of Headgroup on the Physicochemical Properties of Phospholipid Bilayers in Electric Fields: Size Matters. *Langmuir* **2013**, *29*, 1695−1708.
(62) Madrid, E.; Horswell, S. L. Effect of Electric Field on Structure and Dynamics of Bilayers Formed from Anionic Phospholipids. *Electrochim. Acta* **2014**, *146*, 850−860.
(63) Burgess, I.; Szymanski, G.; Li, M.; Horswell, S. L.; Lipkowski, J.; Majewski, J.; Satija, S. Influence of the Electric Field on a Bio-mimetic Film Supported on a Gold Electrode. *Colloids Surf., B* **2005**, *40*, 117−122.
(64) Hillman, A. R.; Ryder, K. S.; Madrid, E.; Burley, A. W.; Wiltshire, R. J.; Merotra, J.; Grau, M.; Horswell, S. L.; Glidle, A.; Dalgliesh, R. M.; Hughes, A.; Cubitt, R.; Wildes, A. Structure and Dynamics of Phospholipid Bilayer Films Under Electrochemical Control. *Faraday Discuss.* **2010**, *145*, 357−379.
(65) Duncan, S. L.; Larson, R. G. Comparing Experimental and Simulated Pressure-Area Isotherms for DPPC. *Biophys. J.* **2008**, *94*, 2965−2986.
(66) Miyoshi, T.; Kato, S. Detailed Analysis of the Surface Area and Elasticity in the Saturated 1,2-Diacylphosphatidylcholine/Cholesterol Binary Monolayer System. *Langmuir* **2015**, *31*, 9086−9096.
(67) Madrid, E. Ph.D. Thesis, University of Birmingham, 2011.
(68) Richer, J.; Lipkowski, J. Measurement of Physical Adsorption of Neutral Organic Species at Solid Electrodes. *J. Electrochem. Soc.* **1986**, *133*, 121−128.
(69) Haiss, W.; Lackey, D.; Sass, J. K.; Besocke, K. H. Atomic Resolution Scanning Tunneling Microscopy Images of Au(111) Surfaces in Air and Polar Organic-Solvents. *J. Chem. Phys.* **1991**, *95*, 2193−2196.
(70) Optical constants and Fresnel 1 software written by V., Zamlynny. Email: Vlad.Zamlynny@AcadiaU.ca.
(71) Jackson, R.; Zamlynny, V. Optimization of Electrochemical Infrared Reflection Absorption Spectroscopy Using Fresnel Equations. *Electrochim. Acta* **2008**, *53*, 6768−6777.
(72) Zamlynny, V.; Lipkowski, J. *Diffraction and Spectroscopic Methods in Electrochemistry*; Alkire, R. C.; Kolb, D. M.; Lipkowski, J.; Ross, P. N., Eds.; Wiley-VCH: New York, 2006; Chapter 9.
(73) Damaskin, B. B.; Petrii, O. A.; Batrakov, V. V. *Adsorption of Organic Compounds on Electrodes*; Nauka: Moscow, 1968.
(74) Guidelli, R.; Aloisi, G.; Becucci, L.; Dolfi, A.; Moncelli, M. R.; Buoninsegni, F. T. Bioelectrochemistry at Metal | Water Interfaces. *J. Electroanal. Chem.* **2001**, *504*, 1−28.
(75) Madrid, E.; Horswell, S. L. The Electrochemical Phase Behaviour of Chemically Asymmetric Lipid Bilayers. *J. Electroanal. Chem.* **2018**, *819*, 338−346.
(76) Lipkowski, J.; Stolberg, L. *Adsorption of Molecules at Metal Electrodes*; Lipkowski, J.; Ross, P. N., Eds.; VCH: New York, 1992; pp 171−238.
(77) Oliynyk, V.; Kaatze, U.; Heimburg, T. Defect formation of lytic peptides in lipid membranes and their influence on the thermodynamic properties of the pore environment. *Biochim. Biophys. Acta, Biomembr.* **2007**, *1768*, 236−245.
(78) Vakurov, A.; Galluzzi, M.; Podestà, A.; Gamper, N.; Nelson, A. L.; Connell, S. D. A. Direct Characterization of Fluid Lipid Assemblies on Mercury in Electric Fields. *ACS Nano* **2014**, *8*, 3242−3250.
(79) Casal, H.; Mantsch, H. H. Polymorphic Phase Behaviour of Phospholipid Membranes Studied by Infrared Spectroscopy. *Biochim. Biophys. Acta, Rev. Biomembr.* **1984**, *779*, 381−401.
(80) Casal, H. L.; Mantsch, H. H. The Thermotropic Phase Behavior of N-Methylated Dipalmitoylphosphatidylethanolamines. *Biochim. Biophys. Acta, Biomembr.* **1983**, *735*, 387−396.
(81) Cameron, D. G.; Casal, H. L.; Mantsch, H. H. Characterization of the Pretransition in 1,2-Dipalmitoyl-sn-glycero-3-phosphocholine by Fourier Transform Infrared Spectroscopy. *Biochemistry* **1980**, *19*, 3665−3672.
(82) Snyder, R. G.; Liang, G. L.; Strauss, H. L.; Mendelsohn, R. IR Spectroscopic Study of the Structure and Phase Behavior of Long-Chain Diacylphosphatidylcholines in the Gel State. *Biophys. J.* **1996**, *71*, 3186−3198.
(83) Umemura, J.; Cameron, D. G.; Mantsch, H. H. A Fourier Transform Infrared Spectroscopic Study of the Molecular Interaction of Cholesterol with 1,2-Dipalmitoyl-sn-glycero-3-phosphocholine. *Biochim. Biophys. Acta, Biomembr.* **1980**, *602*, 32−44.
(84) Mantsch, H. H.; McElhaney, R. M. Phospholipid Phase Transitions in Model and Biological Membranes as Studied by Infrared Spectroscopy. *Chem. Phys. Lipids* **1991**, *57*, 213−226.
(85) Okamura, E.; Umemura, J.; Takenaka, T. Fourier-Transform Infrared-Attenuated Total Reflection Spectra of Dipalmitoylphosphatidylcholine Monomolecular Films. *Biochim. Biophys. Acta, Biomembr.* **1985**, *812*, 139−146.
(86) Snyder, R. G.; Hsu, S. L.; Krimm, S. Vibrational-Spectra in C−H Stretching Region and Structure of Polymethylene Chain. *Spectrochim. Acta, Part A* **1978**, *34*, 395−406.
(87) Umemura, J.; Kamata, T.; Kawai, T.; Takenaka, T. Quantitative Evaluation of Molecular Orientation in thin Langmuir−Blodgett Films by FT-IR Transmission and Reflection−Absorption Spectroscopy. *J. Phys. Chem. A* **1990**, *94*, 62−67.

https://doi.org/10.1021/acs.langmuir.1c01975
Langmuir 2021, 37, 11887−11899

(88) Madrid, E.; Horswell, S. L. Effect of Deuteration on Phase Behavior of Supported Phospholipid Bilayers: a Spectroelectrochemical Study. *Langmuir* **2015**, *31*, 12544−12551.
(89) Cameron, D. G.; Casal, H. L.; Gudgin, E.; Mantsch, H. H. The Gel Phase of Dipalmitoyl Phosphatidylcholine. An Infrared Characterization of the Acyl Chain Packing. *Biochim. Biophys. Acta, Biomembr.* **1980**, *596*, 463−467.
(90) Watkins, E. B.; Miller, C. E.; Liao, W-P.; Kuhl, T. L. Equilibrium or Quenched: Fundamental Differences Between Lipid Monolayers, Supported Bilayers, and Membranes. *ACS Nano* **2014**, *8*, 3181−3191.
(91) Le Bihan, T.; Pezolet, M. Study of the Structure and Phase Behavior of Dipalmitoylphosphatidylcholine by Infrared Spectroscopy: Characterization of the Pretransition and Subtransition. *Chem. Phys. Lipids* **1998**, *94*, 13−33.
(92) Fringeli, U. P. The Structure of Lipids and Proteins Studied by Attenuated Total Reflection (ATR) Infrared Spectroscopy. II. Oriented Layers of a Homologous Series: Phosphatidylethanolamine to Phosphatidylcholine. *Z. Naturforsch. C* **1977**, *32*, 20−45.
(93) Ishioka, T.; Yan, W.; Strauss, H. L.; Snyder, R. G. Normal Mode Analyses of Methyl Palmitate All-Trans and Disordered Forms in Wagging Progressive Region. *Spectrochim. Acta, Part A* **2003**, *59*, 671−680.
(94) Blume, A.; Hubner, W.; Messer, G. Fourier Transform Infrared Spectroscopy of $^{13}C{=}O$-Labeled Phospholipids Hydrogen Bonding to Carbonyl Groups. *Biochemistry* **1988**, *27*, 8239−8249.
(95) Lewis, R. N. A. H.; McElhaney, R. N.; Pohle, W.; Mantsch, H. H. Components of the Carbonyl Stretching Band in the Infrared spectra of Hydrated 1,2-Diacylglycerolipid Bilayers: a Reevaluation. *Biophys. J.* **1994**, *67*, 2367−2375.

https://doi.org/10.1021/acs.langmuir.1c01975
Langmuir 2021, 37, 11887−11899